Multiple Valley Couplings in Nanometer Si MOSFETs

Hui-Xiong Deng, Xiang-Wei Jiang, Jun-Wei Luo, Shu-Shen Li, and Jian-Bai Xia

State Key Laboratory for Superlattices and Microstructures,

Institute of Semiconductors, Chinese Academy of Sciences,

P. O. Box 912, Beijing 100083, China

Lin-Wang Wang*

Computational Research Division, Lawrence

Berkeley National Laboratory, Berkeley, CA 94720

Abstract

We investigate the couplings between different energy band valleys in a MOSFET device using self-consistent calculations of million-atom Schrödinger-Poisson Equations. Atomistic empirical pseudopotentials are used to describe the device Hamiltonian and the underlying bulk band structure. The MOSFET device is under nonequilibrium condition with a source-drain bias up to 2V, and a gate potential close to the threshold potential. We find that all the intervalley couplings are small, with the coupling constants less than 3 meV. As a result, the system eigenstates derived from different bulk valleys can be calculated separately. This will significantly reduce the simulation time, because the diagonalization of the Hamiltonian matrix scales as the third power of the total number of basis functions.

PACS numbers:

*Electronic address: lwwang@lbl.gov

I. INTRODUCTION

As the size of MOSFET (metal-oxide-semiconductor field-effect transistor) shrinks down to nanometer scale [1], quantum mechanical effects become important in describing the physical properties of such devices [2, 3]. In recent years, there have been many developments [4–6] for new computational approaches to simulate the physics of such nanometer devices beyond the traditional semiclassical Drift-Diffusion model. The most direct method is to solve the coupled Schrodinger-Poisson equations. While the Schrodinger's equation treats quantum mechanical effects directly, the Poisson equation yields a self-consistent potential based on the carrier charge density. There are different approximations to describe the Schrodinger's equation. These include the effective mass approximation (EMA) [7, 8], the $\mathbf{k}\cdot\mathbf{p}$ method [9] and the empirical tight-binding model [10]. While the EMA and $\mathbf{k}\cdot\mathbf{p}$ model are widely used, they have several fundamental flaws. One is the questionable validity of the parabolic approximation of the band structure, another is the lack of intervalley coupling in these models. In the conduction band of Si, there are three X valleys with the same energy. Thus, it is quite possible that one needs to solve these valleys together to account for their possible coupling. When the source drain bias potential in a MOSFET is about 1V, the L valley energy at the drain side is similar to the X valley energy at the source side. Thus, it is possible that a X valley electron from the source will coupled to (or tunnel into) the L valley electron at the drain. In the simple effective mass treatment, there is no valley coupling in the Hamiltonian. Different valleys have to be treated separately. To address the importance of intervalley coupling, in this paper we present a MOSFET simulation based on empirical pseudopotential method (EPM) and linear combination of bulk band (LCBB) [11, 12] solutions of the Schrodinger's equation. Our EPM Hamiltonian provides the whole band structure with all band structure valleys, while the LCBB calculation allows solutions of million atom systems. Fig.1 shows the Si band structure calculated using our EPM. As can be seen, the L point is only 1.0 eV higher than X point. Thus, when the bias is larger than 1.0 V, the X point bulk energy at the source side is similar to the L point bulk energy at the drain side. Thus, an intervalley coupling might become important. One of the advantages of the LCBB method is that it allows the selective inclusion of the physically important bulk basis states. Therefore by selecting basis states from different valleys, the valley coupling problem can be studied systematically [13]. We will study the Γ-X, L-X,

X-X couplings, their magnitudes and their effects on the electronic structures of nanosize MOSFETs.

II. MODEL AND CALCULATION

We will investigate a n type channel Si MOSFET with a channel (in the x direction) length of 25 nm and SiO_2 thickness of 1.5 nm. The geometry of the device is shown in Fig.2(a), where the dashed line box is the actual calculation region, which has a length of 25nm in horizontal x direction, a width of 25nm in horizontal y direction, and a height of 27nm in vertical z direction. Doping density in the substrate(which is p type) is $10^{19} cm^{-3}$, and we assume a continuous uniform doping profile in the substrate.

In our approach, we solve self-consistently the coupled Schrödinger-Poisson Equations constructed as

$$(-\frac{1}{2}\nabla^2 + V_b(\mathbf{r}) + V_{str}(\mathbf{r}) + V_{ext}(\mathbf{r}))\psi_i(\mathbf{r}) = E_i\psi_i(\mathbf{r}) \quad (1)$$

$$\nabla[\varepsilon(\mathbf{r})\nabla\phi(\mathbf{r})] = -4\pi[p(\mathbf{r}) - n(\mathbf{r}) + N_d^+(\mathbf{r}) - N_a^-(\mathbf{r})] \quad (2)$$

where $V_b(\mathbf{r}) = \sum_{\mathbf{R}} \upsilon(|\mathbf{r}\text{-}\mathbf{R}|)$, $\upsilon(|\mathbf{r}|)$ is a screened spherical atomic empirical pseudopotential [11] fit to the bulk Si band structure and electron wavefunctions. $\mathbf{R}$ denotes the positions of the atoms. $V_{str}(\mathbf{r})$ is a confinement potential representing the geometry of the device and the band alignment between the bulk Si and SiO_2 layer. Thus, for a given device geometry $V_{str}(\mathbf{r})$ is fixed, independent of the gate voltage and source-drain bias. $V_{ext}(\mathbf{r}) = e\phi(\mathbf{r})$ is the self-consistent electrostatic potential solved from Eq(2). $\varepsilon(\mathbf{r})$ is the position-dependent dielectric constant, 3.9 for SiO_2 and 11.8 for Si. The densities of hole $p(\mathbf{r})$ and ionized donors (acceptors) $N_d^+(\mathbf{r})$ ($N_a^-(\mathbf{r})$) are calculated by a semiclassical approximation [14] for a given potential $\phi(\mathbf{r})$ at room temperature. $n(\mathbf{r})$ is the occupied electron density. The LCBB method [11] is used to solve the eigenstates $\{\psi_i(\mathbf{r}), E_i\}$ of Eq.(1) within the dashed line box of Fig.2(a) containing 0.85 million atoms. The solved eigenstates $\psi_i(\mathbf{r})$ are evaluated on a $104 \times 46 \times 100$ numerical grid in real space, and the occupied n type carrier density n($\mathbf{r}$) on this grid will be calculated (using formula given below) from $\{\psi_i(\mathbf{r}), E_i\}$. Then Eqs. (1) and (2) are solved self-consistently until convergence is reached using a Pulay DIIS (direct inversion of iteration space) potential mixing iterative scheme [15]. The Poisson equation [Eq.(2)] is solved in the region within the dashed line box of Fig.2(a). A fixed potential boundary condition is used at the gate, source and drain areas, and surface parallel and

normal electric field conditions are used at the two lower sides [blue region in Fig.2(a)] and the bottom of the box, respectively.

Due to the applied source-drain voltage, as shown in Fig.2(a), we have different Fermi levels: E_F^L for the source region and E_F^R for the drain region under nonequilibrium condition. One approximate way to calculate the charge density $n(\mathbf{r})$ is to use E_F^L and E_F^R to occupy the wave function $\psi_i(\mathbf{r})$ separately from the left and right hand sides, then use partition functions to put the left and right hand sides together.This leads to the following formula:

$$n(\mathbf{r}) = 2\sum_i |\psi_i(\mathbf{r})|^2 \frac{W_i^L(\mathbf{r}) f_L(E_i) + W_i^R(\mathbf{r}) f_R(E_i)}{W_i^L(\mathbf{r}) + W_i^R(\mathbf{r})}, \tag{3}$$

where $f_{L(R)}(E) = F(E - E_F^{L(R)})$ (F is the Fermi-Dirac distribution function) represents the left (L) and right (R) occupation functions, respectively, and $W_i^L(\mathbf{r})$ and $W_i^R(\mathbf{r})$ are the left and right hand side partition functions for eigenstate $\psi_i(\mathbf{r})$. The partition functions $W_i^{L(R)}$ along the x direction can be described by the WKB approximation on each (y,z) line as $W_i^L(x,y,z) = exp[-2\int_0^x f'(E_c(x,y,z) - E_i)dx]$ and $W_i^R(x,y,z) = exp[2\int_{L_c}^x f'(E_c(x,y,z) - E_i)dx]$. Here $f'(u) = \sqrt{2m_e u}$ (for $u > 0$) and $f'(u) = 0$ (for $u \leq 0$), m_e is the effective mass of the conduction band, and $E_c(x,y,z)$ is the energy of bulk conduction band minimum at point $\mathbf{r} = (x,y,z)$ under a given electrostatic potential $\phi(\mathbf{r})$. Further details of the simulation can be found in Ref.5.

III. RESULTS AND DISCUSSIONS

In the LCBB method, the single-particle wave function ψ_i in Eq.(1) is expanded in terms of Bloch states of the bulk Si:

$$\psi_i(\mathbf{r}) = \sum_n^{N_b} \sum_{\mathbf{k}}^{N_k} C_{n,\mathbf{k}}^i \phi_{n,\mathbf{k}}(\mathbf{r}), \tag{4}$$

where N_b, N_k are the numbers of the bulk bands and k points respectively. $\phi_{n,\mathbf{k}}(\mathbf{r}) = \frac{1}{\sqrt{N}} u_{n,\mathbf{k}}(\mathbf{r}) e^{i\mathbf{k}\cdot\mathbf{r}}$, $u_{n,\mathbf{k}}(\mathbf{r})$ is bulk Bloch state which is described by plane wave functions as $u_{n,\mathbf{k}}(\mathbf{r}) = \frac{1}{\sqrt{V_0}} \sum_{\mathbf{G}}^{N_G} A_{k,n}(\mathbf{G}) e^{i\mathbf{G}\cdot\mathbf{x}}$, N_G is the number of zinc-blende reciprocal-lattice vectors $\mathbf{G}$ within an energy cutoff.

Within the LCBB formalism, the Hamiltonian matrix elements can be written as:

$$< \phi_{n',\mathbf{k}'}|\hat{H}|\phi_{n,\mathbf{k}} >= \Omega_0 \sum_{\mathbf{G},\mathbf{G}'} A_{\mathbf{k}',n'}(\mathbf{G}')[\frac{\hbar}{2m}|\mathbf{k}+\mathbf{G}|^2\delta_{\mathbf{k},\mathbf{k}'}\delta_{\mathbf{G},\mathbf{G}'} + V_{str-ext}(\mathbf{k}-\mathbf{k}')\delta_{\mathbf{G},\mathbf{G}'} + V(|\mathbf{k}+\mathbf{G}-\mathbf{k}'-\mathbf{G}'|^2)e^{-i\mathbf{d}^0\cdot(\mathbf{k}+\mathbf{G}-\mathbf{k}'-\mathbf{G}')}W^0(\mathbf{k}-\mathbf{k}')]A_{\mathbf{k},n}(\mathbf{G}), \quad (5)$$

where Ω_0 is the supercell volume and $\upsilon(q_2)$ is the Fourier transform of $\upsilon(|\mathbf{r}|)$. $\mathbf{d}^0$ is the displacement of atom inside the primary cell $\mathbf{R}$, and $W^0(\mathbf{k})$ is a structure factor $W^0(\mathbf{k}) = \frac{1}{\Omega_0}\sum_{\mathbf{R}_0} W(\mathbf{R}_0)e^{i\mathbf{k}\cdot\mathbf{R}_0}$, where $W(\mathbf{R_0})$ indicates the atomic weight at the atomic site $\mathbf{R_0}$. $V_{str-ext}(\mathbf{k})$ is the Fourier transform of $V_{str}(\mathbf{r}) + V_{ext}(\mathbf{r})$. The last two terms in the right hand side of Eq.(5) describe the intervalley couplings. The amplitudes of these couplings depend critically on the symmetry and atomic details of V($\mathbf{r}$) [11]. Obviously, the bulk potential V_b will not introduce intervalley coupling. The coupling is introduced from both V_{str} and V_{ext}. While the V_{str} introduces coupling for $\Delta\mathbf{k} = \mathbf{k}' - \mathbf{k}$ in the z direction, V_{ext} introduces coupling for $\Delta\mathbf{k}$ in both z and x directions. Additionally, V_{ext} depends on the gate voltage and source-drain bias. The calculation of Hamiltonian matrix elements of Eq(5) is based on a fast algorithm, with the resulting matrix then directly diagonalized to yield the coefficients $C^i_{n,\mathbf{k}}$ of Eq.(4) and eigenenergies E_i of Eq.(1). Here we can separate Eq.(4) into its components:

$$\psi_i(\mathbf{r}) = \sum_n^{N_b}\{\sum_{\mathbf{k}_X}^{N_{k_X}} C^i_{n,\mathbf{k}_X}\phi_{n,\mathbf{k}_X}(\mathbf{r}) + \sum_{\mathbf{k}_\Gamma}^{N_{k_\Gamma}} C^i_{n,\mathbf{k}_\Gamma}\phi_{n,\mathbf{k}_\Gamma}(\mathbf{r}) + \sum_{\mathbf{k}_L}^{N_{k_L}} C^i_{n,\mathbf{k}_L}\phi_{n,\mathbf{k}_L}(\mathbf{r})\}. \quad (6)$$

The k-point sum runs over the supercell reciprocal lattices $\mathbf{k}_X$, $\mathbf{k}_\Gamma$ and $\mathbf{k}_L$ within pockets near X,Γ and L points, as shown in Fig.2(b).$N_k = N_{k_X} + N_{k_\Gamma} + N_{k_L}$. We can define a special $\mathbf{k}^*$ point weight function, $P^i_{\mathbf{k}^*} = \sum_{\mathbf{k}\in\mathbf{k}^*}\sum_n |C^i_{n,\mathbf{k}}|^2$, for a given eigensate subject to

$$P_X(E_i) + P_\Gamma(E_i) + P_L(E_i) = 1 \quad (7)$$

due to wavefunction normalization. We can use these weights to characterize each eigenstate and to analyze valley coupling within each eigenstate. For the Si-MOSFET studied here, in equilibrium condition (i.e., zero drain-source bias: $V_{ds} = 0.0V$), the weights of wave functions mainly come from the first term of Eq.(6) for all the eigenstates since the conduction-band minimum (CBM) of the bulk Si is localized in the X-valley. In this case, all the Γ-X and

L-X intervalley couplings effects are small. In the nonequilibrium conditions, when a large source-drain bias potential exists, Γ-X and L-X intervalley couplings can play significant roles since they can have similar energies from the different parts of the device. In the following, we will study these situations.

To explore Γ-X coupling, we have chosen two conduction bands [$N_b = 2$ in Eq(4)] at each k-point, and selected 1468 k-points at each of the three non-equivalent X-valleys (X_{001}, X_{010}, X_{100}) and 1213 k-points at the Γ-valley. This amounts to 5617 total k-points. To study the L-X coupling, we have chosen 1468 k-points at each of the three non-equivalent X-valleys (X_{001},X_{010}, X_{100}) and 587 k-points at each of the two L-valleys ($L(111)$,$L(11-1)$). This amounts to 5578 total k-points. The other two L points ($L(1-11)$,$L(1-1-1)$) are not included to reduce the size of the basis set. However, since they are physically equivalent to $L(111)$ and $L(11-1)$, and we are only interested in L-X coupling, not L-L coupling, this does not affect our conclusions. The resulting LCBB calculated valley weight functions P_Γ and P_L for different eigenstates are shown in Fig.3 for V_{ds}=2.0 and $Vg = 2.4V$ (slightly larger than the threshold gate potential of 2.1V). The energies in the horizontal axis of Figs.3-6 are measured from the vacuum level which is fixed in an EPM Hamiltonian. As can be seen in Fig.3(a), P_Γ is very small in the whole energy range, indicating that the contributions of the Γ-valley to the electronic states are always very small. Fig.3(b) shows that P_L is almost zero for low energy states, but almost one for some higher energy states. This indicates that the eigenstates consist either of pure X point bulk states, or of pure L point bulk states. Thus, there is almost no L-X coupling. However, this does not mean that we can completely ignore the L point contribution. For a strongly biased system, the eigenstates from the L points can be occupied from the drain side. This is demonstrated by the density of state (DOS) of the eigenstates derived purely from L-valley shown in Fig.4. These DOS are calculated by including only the L valley basis set in Eq(6). As we can see, as the V_{ds} increases, the DOS shifts towards Fermi energy E_F^L. When V_{ds}=2.0V, there are already some L-valley derived states which will be occupied. Nevertheless, since the L-X coupling is small, these L-valley derived states can be calculated by using L-valley basis functions alone. The mobile charge density we calculated from the contributions of L-valley electron states is Q_L=$1.2 \times 10^{-22} (\mu C/cm^{-2})$, which is not entirely negligible. Note that, the two other L-valleys $L(1-11)$,$L(1-1-1)$, not included in Fig.4, are equivalent to the two valleys used in Fig.4. So the total L-valley contribution is twice of what shown in Fig.4.

The same state occupation does not happen for the Γ point derived states at $V_{ds} = 2.0V$, since the Γ point has a much higher energy than the L point valley, as shown in Fig.1.

Due to the small X-L coupling, it is plausible that the total DOS (and the corresponding charge density) can be represented as the sum of the DOS from different valleys. To confirm this, Fig.5 compares the DOS calculated with different X and L valley basis set selections with $V_{ds} = 2.0V$ and $V_g = 2.4V$. Blue and the cyan lines represent DOS with X-valley only and L-valley only basis sets, respectively. As shown in Fig.4, a small part of the L-valley DOS is below the Fermi energy E_F^L, hence occupied. We can sum over DOS_X and DOS_L, yielding X+L shown in Fig.5 as the red line. This is compared with the directly calculated total DOS with basis set from both X and L valleys (XL, the solid triangle). We can see that DOS_X+DOS_L is almost exactly the same as DOS_{XL}. Since calculating DOS_X and DOS_L separately is much faster than calculating DOS_{XL} due to the cubic scaling of the matrix diagonalization, our result has an important implication for the future MOSFET simulations: there is no need to calculate the wavefunctions using all valley basis functions together, instead the contributions from different valleys can be calculated separately.

We next investigate the couplings between three X valleys: X_{001}, X_{010}, X_{100}. These three valleys are nonequivalent due to the device geometry (Fig.2). In Fig.6, we show the DOS of the individual X-valleys, their sum, and the total DOS calculated with three X-valley basis sets together. We find that the direct sum of partial $\mathrm{DOS}_{X_{100}}$, $\mathrm{DOS}_{X_{010}}$ and $\mathrm{DOS}_{X_{001}}$ is almost indistinguishable from the total density of state $\mathrm{DOS}_{X_{100,010,001}}$ calculated with all the basis sets. This demonstrates that even the couplings among the three X-valleys are small. Thus for practical purposes, one can calculate the system eigenstates from these three X-valleys separately. Note, the $\mathrm{DOS}_{X_{001}}$ has the lowest energy tail, followed by $\mathrm{DOS}_{X_{100}}$, then by $\mathrm{DOS}_{X_{010}}$. This is because the X_{001} valley has a large effective mass (parallel effective mass of the X-valley) in the vertical z direction (Fig.2(b)). Since the strongest confinement effects happen in the z direction, the corresponding large effective mass produces a small quantum confinement energy, thus it has the lowest eigen states, and lowest DOS tail. The X_{100} has a small effective mass (transverse effective mass of the X-valley) in the z direction, but it has a large effective mass in the x direction (Fig.2(b)). Since the x direction also has a quantum confinement effect, it leads to intermediate eigen energies and DOS. In contrast, X_{010} has a small effective mass in both z and x directions, thus it has the largest quantum confinement energy and the highest DOS.

Above, we have analyzed the intervalley couplings by examining the eigenstate wavefunctions and density of states. The intervalley couplings can also be determined directly from the coupling matrix elements $< \phi_{\mathbf{k}'} | \hat{H} | \phi_{\mathbf{k}} >$, where $\mathbf{k}'$ and $\mathbf{k}$ are from different valleys, and $\phi_{\mathbf{k}}$ is the bulk Bloch function at the $\mathbf{k}$ point. The values of these matrix elements are shown in Table.I for different V_{ds} and V_g situations. We have the following observations: (i) In general, the coupling matrix elements are all very small. The largest is about 3 meV. Thus, for all practical purposes for device simulation, we can ignore the intervalley coupling, and calculate the device eigenstates from different valleys separately. This is the main conclusion of this paper. (ii) When $\mathbf{k}' - \mathbf{k}$ has a nonzero component in the [010] direction (y direction in Fig.2), the coupling constant is zero. This is because in the y direction, the device is periodic with a primary cell unit. Thus any $\mathbf{k}' - \mathbf{k}$ component in this direction which is not a multiple of the reciprocal lattice of the primary cell will lead to a zero integral in the matrix element. This rule makes all the possible L-X couplings to be zero (including the other two L points not shown in Table.I). This might seem contradictory to the results shown in Fig.3(b). There, although the L-X coupling is small, it is nevertheless not exactly zero. However, P_L is much smaller than P_Γ, despite the fact that the band energy of the X point is much closer to the L point than to the Γ point. The small remaining P_L in Fig.3(b) comes from the k-points slightly off the exact X and L points, which can have zero [010] $\mathbf{k}' - \mathbf{k}$ components, thus allowing coupling between them. Note that, in this paper, we have used a uniform continuous doping model. If the atomistic random dopant positions are considered, the coupling will not be zero between any two valleys. Nevertheless, such random potential induced coupling constant will also be small, on the order of a few meV, as demonstrated by the alloy study in Ref.16.

IV. CONCLUSION

We have studied the invervalley coupling in a nanometer sized MOSFET. We find that the intervalley coupling is small in general, on the order of a few meV. As a result, the eigenstates derived from different valleys can be calculated separately without considering intervalley couplings. In terms of coupling amplitudes, the X-Γ coupling is larger than the X-L coupling. At the exact valley center, the X-L coupling is zero. The X-X coupling has the largest amplitude of about 3 meV.

V. ACKNOWLEDGMENTS

This work was supported by the National Natural Science Foundation of China (Grant Nos. 60521001 and 60776061). The work by L.W.Wang is funded by the DMSE/BES/SC of the U.S.Department of Energy under Contract No. DE-AC02-05CH11231.

VI. REFERENCES

[1] International Technology Roadmap for Semiconductors. Available at http://public.itrs.net.

[2] M. Ieong, B. Doris, J. Kedzierski, K, Rim, and M. Yang, Science **306**, 2057 (2004).

[3] Y. Taur, IBM J. Res. & Dev. **46**, 213 (2002), and reference therein; Y. Taur, D. A. Buchanan, W. Chen, D. J. Frank, K. E. Ismail, S. H. Lo, G. A. Sai-Halasz, R. G. Viswanathan, H. -J. C. Wann, S. J. Wind, and H. -S. Wong, Proc. IEEE, **85**, 486 (1997).

[4] J.-H. Rhew and M. S. Lundstrom, J.APPl.Phys. **92**, 5196 (2002).

[5] J. W. Luo, S. S. Li, J. B. Xia, and L. W. Wang, Appl. Phys. Lett **90**, 143108 (2007).

[6] A. Asenov, G. Slavcheva, A. R. Brown, J. H. Davies, and S. Saini, IEEE Trans, Electron Dev, Vol. **48**, No. 4, pp. 722-729, 2001.

[7] G. Curatola, G. Fiori, and G. Iannaccone,Solid-State Electron. **48**, 581 (2004).

[8] J. Wang, E. Polizzi, and M. S. Lundstrom, J.Applied.Phys. **96**, 2192 (2004).

[9] L. W. Wang and A. Zunger, Phys. Rev. B **54**, 11417 (1996).

[10] M. Bescond, J. L. Autran, D. Munteanu, and M. Lannoo,Solid-State Electron. **48**, 567 (2004).

[11] L. W. Wang and A. Zunger, Phys. Rev. B **59**, 15806 (1999).

[12] J. W. Luo, S. S. Li, J. B. Xia, and L. W. Wang, Appl. Phys. Lett. **88**, 143108 (2006).

[13] L. W. Wang, A. Franceschetti, A. Zunger, Phys. Rev. Lett. **78**, 2819 (1997).

[14] S. M. Sze,*Physics of Semiconductor Devices,* 2nd ed.(Wiley, New York, 1981).

[15] G. Kresse and J. Furthmuller, Phys. Rev. B **54**, 11169 (1996).

[16] L. W. Wang and A. Zunger, Phys. Rev. B **56**, 12395 (1997).

TABLE I: Magnitudes (in meV) of single-k-point coupling matrix element $< \phi_{\mathbf{k}'} | \hat{H} | \phi_{\mathbf{k}} >$ calculated using LCBB method for different V_{ds} and V_g conditions. $\mathbf{\Delta k}$ represents $\mathbf{k}'$-$\mathbf{k}$ folded into the First Brillouin Zone.

$\mathbf{k}' \longrightarrow \mathbf{k}$	$\mathbf{\Delta k}$	$V_{ds} = 0.0(V)$ $V_g = 2.4(V)$	$V_{ds} = 0.0(V)$ $V_g = 2.8(V)$	$V_{ds} = 1.0(V)$ $V_g = 2.4(V)$	$V_{ds} = 2.0(V)$ $V_g = 2.4(V)$
$X_{100} - L_{111}$	$(\frac{\pi}{a}, -\frac{\pi}{a}, -\frac{\pi}{a})$	0	0	0	0
$X_{010} - L_{111}$	$(-\frac{\pi}{a}, \frac{\pi}{a}, -\frac{\pi}{a})$	0	0	0	0
$X_{001} - L_{111}$	$(-\frac{\pi}{a}, -\frac{\pi}{a}, \frac{\pi}{a})$	0	0	0	0
$X_{100} - \Gamma$	$(\frac{2\pi}{a}, 0, 0)$	0.0084	0.0075	0.697	1.42
$X_{010} - \Gamma$	$(0, \frac{2\pi}{a}, 0)$	0	0	0	0
$X_{001} - \Gamma$	$(0, 0, \frac{2\pi}{a})$	0.120	0.336	0.087	0.064
$X_{100} - X_{010}$	$(0, 0, \frac{2\pi}{a})$	2.66	2.23	2.62	2.59
$X_{100} - X_{001}$	$(0, \frac{2\pi}{a}, 0)$	0	0	0	0
$X_{010} - X_{001}$	$(\frac{2\pi}{a}, 0, 0)$	0.016	0.014	0.76	1.55
$L_{111} - L_{\bar{1}11}$	$(\frac{2\pi}{a}, 0, 0)$	0.0048	0.0042	0.007	0.010
$L_{111} - L_{1\bar{1}1}$	$(0, \frac{2\pi}{a}, 0)$	0	0	0	0
$L_{111} - L_{11\bar{1}}$	$(0, 0, \frac{2\pi}{a})$	1.78	1.79	1.77	1.77
$L_{\bar{1}11} - L_{1\bar{1}1}$	$(0, 0, \frac{2\pi}{a})$	0.57	0.36	0.55	0.54
$L_{\bar{1}11} - L_{11\bar{1}}$	$(0, \frac{2\pi}{a}, 0)$	0	0	0	0
$L_{1\bar{1}1} - L_{11\bar{1}}$	$(\frac{2\pi}{a}, 0, 0)$	0.0047	0.0043	0.35	0.71

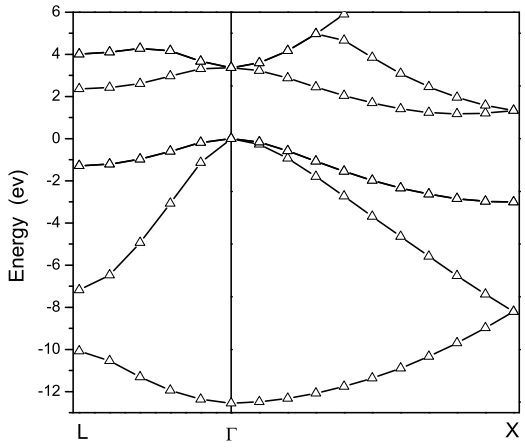

FIG. 1: The Si bulk band structure calculated using our EPM.The top of valence band is at zero energy.

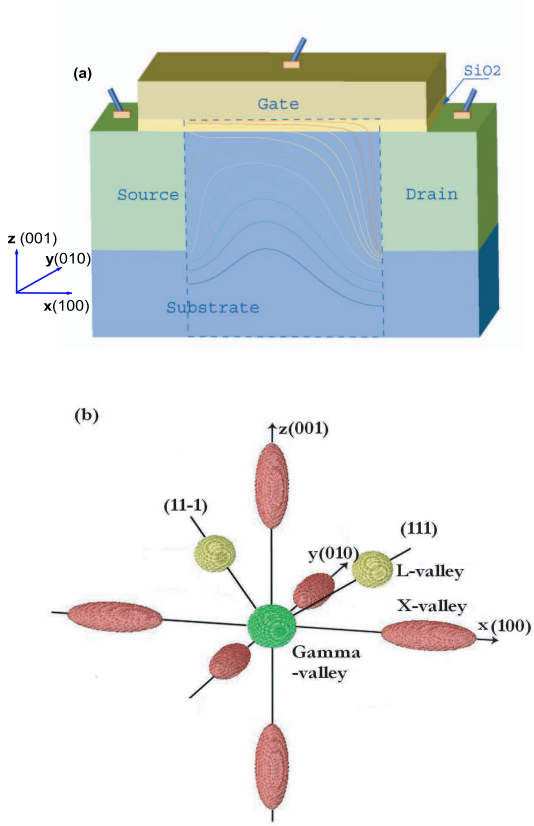

FIG. 2: (color online) (a) Schematic MOSFET structure along with potential contour lines with source-drain voltages. The actual calculation domain is contained in the dashed line box. (b) Schematic k-point distribution chosen by actual calculation in k-space. For clarity, only two L-points (11-1),(111) out of four are illustrated.

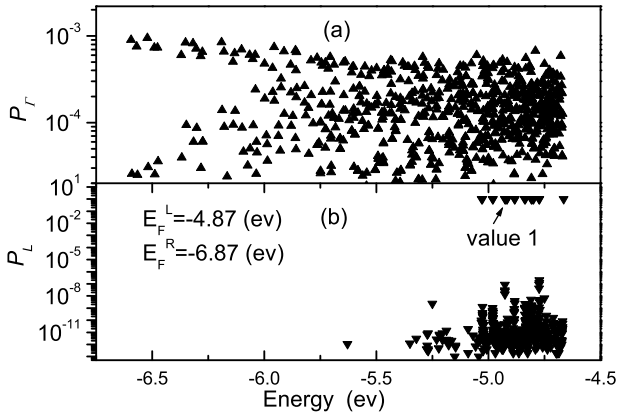

FIG. 3: Probability distribution P_Γ (a) and P_L (b) versus eigenenergies with applied voltages $V_{ds} = 2.0V$ and $V_g = 2.4V$. Each symbol represents one eigenstate,with its eigen energy shown in the horizontal axis. For energies less than -5.75eV, the resulting calculated P_L is zero (or almost zero), thus not shown in our logarithmic coordinate.

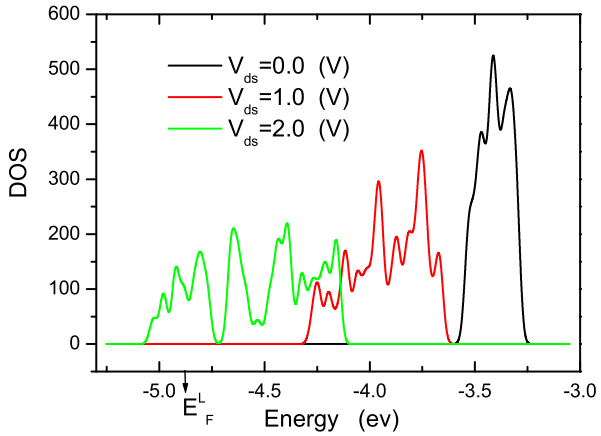

FIG. 4: (color online) Density of states of L-valley (including only $L(111)$,$L(11-1)$) with source-drain voltages $V_{ds} = 0V$(black), $1V$(red), $2V$(green) respectively States lower than E_F^L (indicated by the vertical arrow) will be occupied from the drain side.

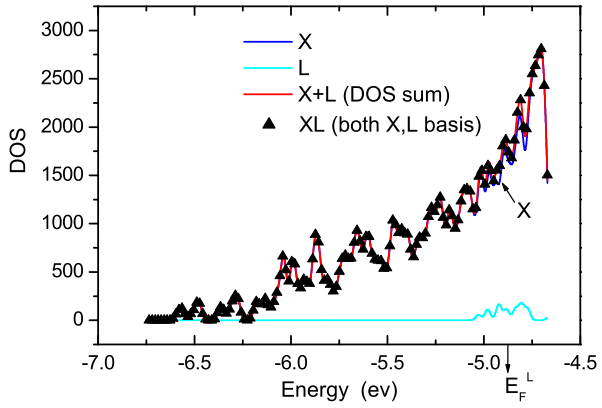

FIG. 5: (color online) Density of states calculated by selecting different valley basis sets with applied voltages $V_{ds} = 2.0V$ and $Vg = 2.4V$.

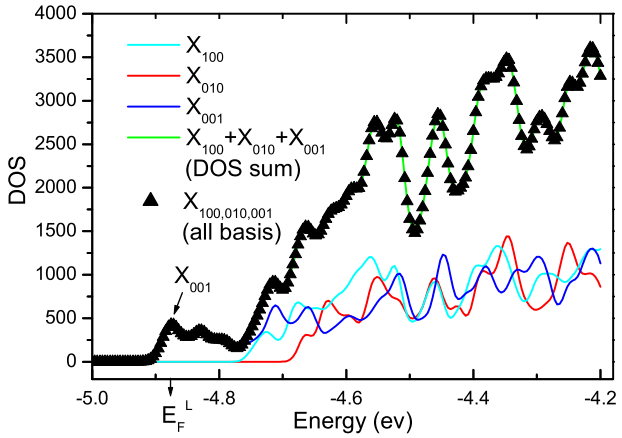

FIG. 6: (color online) Total $\mathrm{DOS}_{X_{100,010,001}}$ (solid triangle) of X-valley and partial $\mathrm{DOS}_{X_{100}}$, $\mathrm{DOS}_{X_{010}}$, $\mathrm{DOS}_{X_{001}}$ in [100](cyan), [010](red), [001](blue) X-valleys, respectively, with applied voltages $V_{ds} = 0V$ and $V_g = 2.4V$. The green line represents the direct sum of partial $\mathrm{DOS}_{X_{100}}$, $\mathrm{DOS}_{X_{010}}$ and $\mathrm{DOS}_{X_{001}}$. For $V_{ds} > 0$, we find the same agreement between X_{100}+X_{010}+X_{001} and $X_{100,010,001}$.